Supplementary Information

For

Measurements of electrically tunable refractive index of MoS_2 monolayer and its usage in optical modulators

Vasyl G. Kravets[1], Fan Wu[1,2,3], Gregory H. Auton[4], Tongcheng Yu[1], Shinji Imaizumi[1,5], Alexander N. Grigorenko[1]

[1]School of Physics and Astronomy, the University of Manchester, Manchester, M13 9PL, UK

[2] Key Laboratory for Non-Equilibrium Synthesis and Modulation of Condensed Matter (Ministry of Education), School of Science, Xi'an Jiaotong University, Xi'an, Shaanxi 710049, China

[3] School of Textile Science and Engineering, Xi'an Polytechnic University, Xi'an, Shaanxi 710048, China

[4] National Graphene Institute, University of Manchester, Manchester M13 9PL, UK

[5] Fundamental Technology Research and Development Division 2 R&D Center Sony Corporation, Atsugi Tec. 4-14-1 Asahi-cho, Atsugi 243-0014, Japan

Sample fabrication. Samples were fabricated using electron beam deposition, chemical vapour deposition, etching procedure and 2D material transfer. First, a 3 nm-thick Cr adhesion layer and 65 nm Au film were deposited on top of a 1 mm-thick quartz substrate using electron beam evaporation. Second, a Si_3N_4 waveguide layer was grown by chemical vapor deposition (CVD) to cover the Au film. Third, a monolayer of MoS_2 (grown by the CVD method on Si/SiO_2 substrate and acquired from 2D Semiconductors) was spin coated with a poly(methyl methacrylate) (PMMA) resist. Then, the $PMMA/MoS_2/SiO_2/Si$ stacks were set onto the scotch type with a window and floated in KOH solution until complete

Si/SiO_2 etching which happened within a few hours. Next, the PMMA/MoS_2 films on the scotch type were rinsed with DI water and fished for transfer procedure. Fourth, the resulting monolayer of MoS_2 was transferred on top of quartz/Au/Si_3N_4 structure using the standard dry-transfer technique as described in [S1]. Finally, after drying overnight, the samples were baked on a heating plate at 120^{o}C for 20 min in order to improve MoS_2 adhesion to the Si_3N_4 layer and the PMMA layer was removed by soaking in acetone.

Characterisation. Raman and photoluminescence (PL) spectra of the CVD grown MoS_2 monolayer was recorded with a Witec confocal Raman spectrometer at the excitation wavelengths of 514nm and 632.8nm. Fourier Transform Infra-Red (FTIR) spectroscopy was performed with the help of a Bruker Vertex 80 system and a Hyperion 3000 microscope. A variety of sources and detectors, combined with aluminium coated reflective optics enable this system to be used from visible to mid-IR wavelengths.

We also performed an accurate determination of the complex refractive index and thickness of a MoS_2 monolayer using a variable angle Woollam M2000F focussed-beam spectroscopic ellipsometer. The spot size on the sample was approximately 30 μm × 80 μm at ~70-80° angles of incidence. Ellipsometry measures two parameters, Ψ (reflection) and Δ (phase), which are related to the complex amplitude reflectance ratio: $\tan(\Psi)\exp(i\Delta) = r_p/r_s$, where r_p and r_s are the amplitude reflection coefficients for *p*- and *s*-polarized light [S2]. In addition to ellipsometric parameters Ψ and Δ, the ellipsometer allowed us to separately measure R_p and R_s, the intensity reflections for *p*- and *s*-polarized light, respectively, at various angles of incidence with respect to the total light intensity. Note that the ellipsometric parameter Ψ simultaneously describes interference resonances excited by *p*-polarized light (TM modes), when r_p and Ψ tend to zero and *s*-polarized light (TE modes) when values of r_s become very small and Ψ goes to 90°.

Raman spectra. Figure S1 shows the Raman spectra of a CVD grown MoS_2 monolayer. Raman spectra were measured from the MoS_2 films placed on different substrates using an excitation laser with wavelength of 514.5 and 632.8 nm. The separation between the in-plane mode (E_{2g}) at 386 cm^{-1} and out-of-plane mode (A_{1g}) at 406 cm^{-1} is 20 cm^{-1} for as-grown film on Si/SiO_2 substrate, which is typical for a monolayer of MoS_2 [S3, S4]. We found that the position of E^1_{2g} peak is insensitive to the underlying layer (SiO_2 or Si_3N_4) with accuracy of ~0.2 cm^{-1} (which is close to the measurement error). However, the frequency of the A_{1g} mode was red shifted by ~3 cm^{-1} for a MoS_2 monolayer transferred to Si_3N_4 film as shown in Fig. S1. This shift could be caused by an additional doping from Si_3N_4 that changes the electron density in MoS_2. Intensities of Raman signals were strongly dependent on local electrical fields on the surface of SiO_2 and Si_3N_4. Optical interference, resulting from reflection and refraction at interfaces MoS_2/Si_3N_4 and Si_3N_4/Au, strongly enhance (about one order of magnitude) the Raman signal as compared to dielectric/dielectric ($Quartz/Si_3N_4$) and dielectric/semiconductor (Si/SiO_2) interfaces. It is worth noting that the intensity ratio between the E^1_{2g} and A_{1g} Raman active modes (I_{E2g}/I_{A1g}) changes from ~1.05 for a $Au/Si_3N_4/MoS_2$ hybrid nanostructure to ~0.5 for a $Si/SiO_2/MoS_2$ one. Therefore, the enhancement of Raman intensity of MoS_2 in the studied hybrid nanostructures could originate from the increase of local electrical fields on the surface of Si_3N_4.

The importance of interference in our structures was confirmed from MoS_2 photoluminescence measured on different substrates (see Fig. S2). The PL emission from the A exciton at ~680 nm was found to depend on geometry of the structure. First, the main PL peak of A exciton was shifted to lower energies in the presence of a gold sublayer. Second, PL intensity was nearly 5 times larger for the Au-based sample than that for a MoS_2 monolayer on the top of $quartz/Si_3N_4$ substrate. PL enhancements have their origin in higher reflectivity of Si_3N_4/Au interface for both excitation and emission wavelengths as compared

to that of Si_3N_4/quartz interface, consistent with the result reported previously [S5]. Third, PL spectra demonstrate a small Stokes shift (about ~50 nm), which is the difference in wavelengths between positions of the PL peak and laser excitation (632.8 nm). The Raman (Fig. S1) and PL (Fig. S2) spectra indicate the excellent optical quality of the MoS_2 monolayer and demonstrate importance of interference effects.

Refractive index of insulator, Si_3N_4 film. The refractive index and dielectric permittivity $\varepsilon_d=n_d^2$ of Si_3N_4 film were determined using ellipsometry measurements. We have carried out optical measurements in a broad spectral region (250-1700 nm). Silicon nitride (Si_3N_4) is a wide bandgap semiconductor material transparent to both visible and infrared light. Our measurements confirm the stoichiometric nature of the deposited Si_3N_4 film. We found that the spectral dependence of the refractive index, n_d, in the 250-1700nm range of Si_3N_4 films of different thicknesses (see Fig. S3), was the same as for a bulk structure described in [S6].

FTIR measurements. The infrared spectra of silicon nitride films exhibit a strong band around 890 cm^{-1} and a shoulder at 1170 cm^{-1}, arising from Si-N vibration (Fig. S4). These results suggest that the film contains the stable Si-N bond which forms the bulk-like network. The strong and sharp mode centred at 890 cm^{-1} shows the formation of a continuous Si_3N_4 film and can be assigned to the transverse optical phonon (TO) mode [S7]. The observed positions of the longitudinal (LO) and TO optical phonon modes in the IR spectra (Fig. S4) indicate that the CVD deposited Si_3N_4 film becomes dense even for small thickness. Observed features at ~2165 and 2360 cm^{-1} most probably correspond to Si-H and SiN_3-H bonds present in the silicon nitride network, which is in good agreement with the data reported for CVD Si_3N_4 films [S7].

Using frequencies of the LO and TO optical phonon modes extracted from FTIR measurement, we can estimate the static dielectric constant, ε_{st} of the CVD deposited Si_3N_4

film. It is well known that the large static dielectric constant can be calculated using the Lyddane-Sachs-Teller formula [S8]:

$$\varepsilon_{st} = \varepsilon_{\infty}\frac{\omega_{LO}^2}{\omega_{TO}^2} \qquad (S1)$$

where ω_{LO} and ω_{TO} are the longitudinal optic and transverse optic phonon frequencies respectively, ε_{∞} is the high frequency permittivity for a Si_3N_4 film evaluated from dependence of the refractive index in the low wavelength region (Fig. S3). Our measurements gave a value of ε_{st}≈8.5 for studied Si_3N_4 films due to the large frequency of the LO mode (ω_{LO} ≈ 1170 cm^{-1}) and the small frequency of the transverse optical mode (ω_{TO} ≈890 cm^{-1}).

Ellipsometric data and optical constants. To retrieve optical constants from ellipsometric measurements, we performed regression fitting of measured spectroscopic ellipsometry data using Fresnel's equations for a multilayer model that consisted of a quartz substrate, a Au layer, a Si_3N_4 layer and a MoS_2 monolayer. The thicknesses of the layers were taken from the experimental geometry and separate modelling, while the optical constant of the sublayer was measured and fitted in separate experiments. The fitting of ellipsometry data was performed using Woollam WVASE32 software. The quartz/Au and quartz/Au/Si_3N_4 structures were also separately measured and modelled using the same software. We started our analysis by determining thickness of the Si_3N_4 layer fabricated on top of quartz/Au substrate using a ellipsometric spectra measured outside the sample area. The thickness of a MoS_2 monolayer was taken to be equal 0.7 nm (as found by additional AFM measurements). Ellipsometric spectra of the Au/Si_3N_4/MoS_2 hybrid waveguide nanostructure are shown in Figure S5. It is worth noting that both Ψ (and Δ which is not shown) demonstrate complicated behaviour due to the interference effect. The ellipsometric functions also show a prominent variability in the vicinity of the A and B exciton absorbance (600-660nm). Measured wavelength dependences

of the complex refractive index ($\tilde{n} = n + ik$) of MoS_2 monolayer for two different gate voltages are shown in Figs. 3 and S6.

The extracted dielectric function, $\varepsilon(\omega)=(n+ik)^2$, of a CVD MoS_2 monolayer can be modelled by fitting with a multi-Lorentzian function [S9]

$$\varepsilon(\omega) = 1 + \sum_{k=1}^{N} \frac{f_k}{E_k^2 - E^2 - iE\gamma_k} \quad , \qquad (S2)$$

where f_k, E_k, and γ_k are the oscillator strength, the spectral resonance energy E_k, and the spectral width γ_k of the k-th oscillator, respectively. These values for the model parameters for a MoS_2 monolayer were determined by fitting Eq. (*S*2) to the experimental data presented in Figs. 3 and S6. A good agreement between the extracted experimental dependences of the complex refractive index ($\tilde{n} = n + ik$) and the analytical formula (*S*2) were obtained for the f_k, E_k, and γ_k parameters presented in the Table I. Note that the numerical fitting is less accurate for short wavelengths due to a possible contribution of film roughness and additional impurities to experimental data and in the IR range where the Drude term needs to be added to multi-Lorentzian function (*S*2). To describe the variation of the refractive index (n and k) with gating voltage, V_g, we change the parameters associated with the excitons A and B. To examine the accuracy of the fitting method, we compared the imaginary part of the refractive index, k, of a MoS_2 monolayer for different gate voltages in Figure S6. The measured and fitted values show nice consistency in the vicinity of A and B exciton peaks as shown in Fig. S6. Note that the resonant energies E_1(A) and E_2(B) for excitons A and B do not change with applied V_g. We found that field-dependence of the refractive index of MoS_2 is caused by a variation of the oscillator strength $f_{1,2}$ and the spectral width $\gamma_{1,2}$ for both excitons (Table 1, Fig. S6). Changes of these parameters could be induced by injected charge carries. Such injection affects the optical properties of the MoS_2 monolayer due to Coulomb scattering and dielectric screening.

Refractive index of a MoS_2 monolayer as a function of gating voltage. Using a Fresnel transfer matrix model of the waveguide hybrid device (Fig. 1) and the measured spectra of the polarized reflectance at different gate voltages (Fig. 3), we were able to extract the dependence of the complex refractive index of a MoS_2 monolayer as a function of gating voltage (induced electron density). In our calculation, we modelled the CVD Si_3N_4 film as a Cauchy film described by three coefficients *A*, *B*, and *C* such that $n_d = A + B/\lambda^2 + C/\lambda^4$, where λ is the wavelength of the incident light. The fitting of the experimental spectroscopic reflection measured on the same Si_3N_4 film outside gold and MoS_2 layers gave the values *A*=1.988, *B*=0.02, *C*=0.0003. Using spectroscopic ellipsometry, we also extracted the complex refractive index of an electron-beam deposited gold film used in our structures modelled by fitting with two Lorentz functions and the Drude term. Calculated values for *p*- and *s*-polarised reflectance corresponding to our experimental design are represented in Fig. 4. A good agreement between experiments and calculations was observed for both polarisations. Our calculations demonstrate that the *s*-polarised reflectance of the studied heterostructure can indeed be electrically tuned in the range of 10-13 % due to injection of charge carriers into the MoS_2 monolayer and the changes in the complex refractive index of MoS_2 resulting from spectral broadening of widths $\gamma_{A,B}$ and the decreasing of oscillator strengths $f_{A,B}$.

Figure S7 shows the calculated *s*-polarised reflection of MoS_2/Si_3N_4/Au nanostructure as a function of the incident wavelength and the thickness of the dielectric Si_3N_4 layer, suggesting that the optimized Si_3N_4 thickness is in the range of 390-415 nm**.**

REFERENCES

S1. Kretinin, A. V., Cao, Y., Tu, J. S., Yu, G. L., Jalil, R., Novoselov, K. S., Haigh, S. J., Gholinia, A., Mishchenko, A., Lozada, M., Georgiou, T., Woods, C. R., Withers, F., Blake, P., Eda, G., Wirsig, A., Hucho, C., Watanabe, K., Taniguchi, T., Geim, A. K., Gorbachev, R. V. Electronic properties of graphene encapsulated with different two-dimensional atomic crystals. *Nano Lett.* **14** (6), 3270–3276 (2014).

S2. Azzam, R. M. A. & Bashara, N.M. *Ellipsometry and Polarized Light* (North-Holland, 1987).

S3. Tonndorf, P., Schmidt, R., Bouttger, P., Zhang, X., Bourner, J., Liebig, A., Albrect, M., Kloc, Ch., Gordan, O., Zahn, D.R.T., de Vasconcellos, S. M., Bratschitsch, R. Photoluminescence emission and Raman response of monolayer MoS_2, $MoSe_2$, and WSe_2. *Opt. Express* **21**, 4908–4916 (2013).

S4. Li, H., Zhang, Q., Yap, C. C. R., Tay, B. K., Edwin, T. H. T., Olivier, A., Baillargeat, D. From bulk to monolayer MoS_2: Evolution of Raman scattering. *Adv. Funct. Mater.* **22***(7)*, 1385–1390 (2012).

S5. Zhang, H., Wan, Y., Ma, Y., Wang, W., Wang, Y., Dai, L. Interference effect on optical signals of monolayer MoS_2, *Appl. Phys. Lett.* **107,** 101904 (2015)**.**

S6**.** Palik, E. D. *Handbook of Optical Constants of Solids* (Academic, San Diego, 1998).

S7. Tsu, D. V., Lucovsky, G., Mantini, M. J. Local atomic structure in thin films of Silicon Nitride and Silicon Diimide produced by remote plasma-enhanced chemical-vapor deposition. *Phys. Rev. B* **33** (10), 7069-7076 (1986).

S8. Kittel, C. *Introduction to Solid State Physics* (Wiley, 2004, 704 p.).

S9. Wooten, F. *Optical Properties of Solids* (Academic Press, New York and London, 1972).

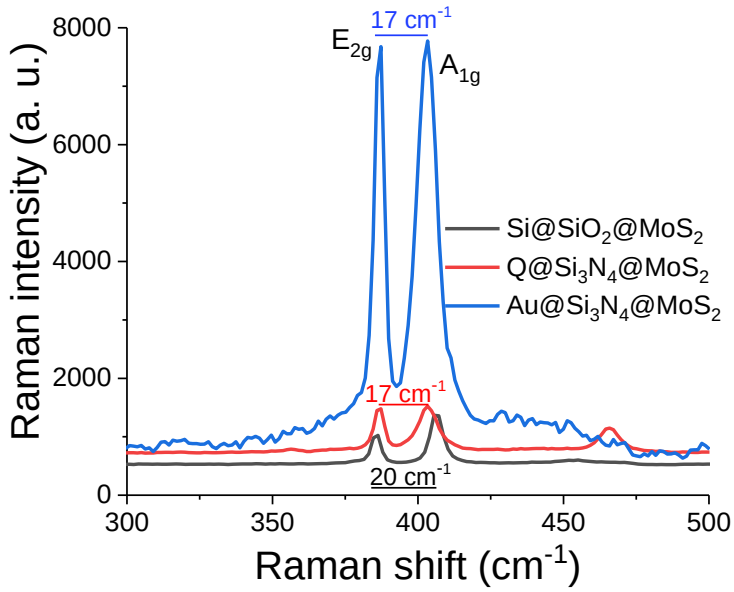

Figure S1. Raman spectra of the MoS_2 monolayer stacked in $Si/SiO_2/MoS_2$ (λ_{exc}=514.5nm; black curve), $Quartz/Si_3N_4/MoS_2$ (red curve), and $Au/Si_3N_4/MoS_2$ (blue curve) nanostructures (for both dependences λ_{exc}=632.8nm).

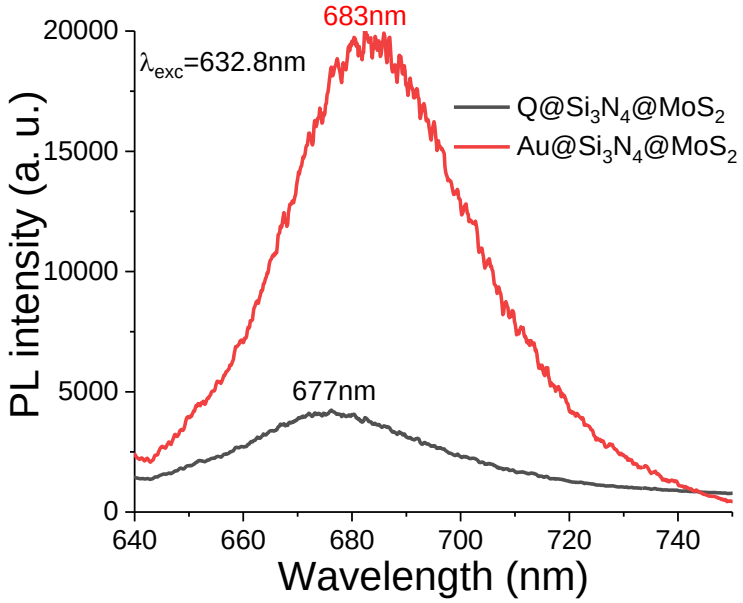

Figure S2. PL spectra of the MoS_2 monolayer stacked in $Quartz/Si_3N_4/MoS_2$ (black curve) and $Au/Si_3N_4/MoS_2$ (red curve) nanostructures (λ_{exc}=632.8nm).

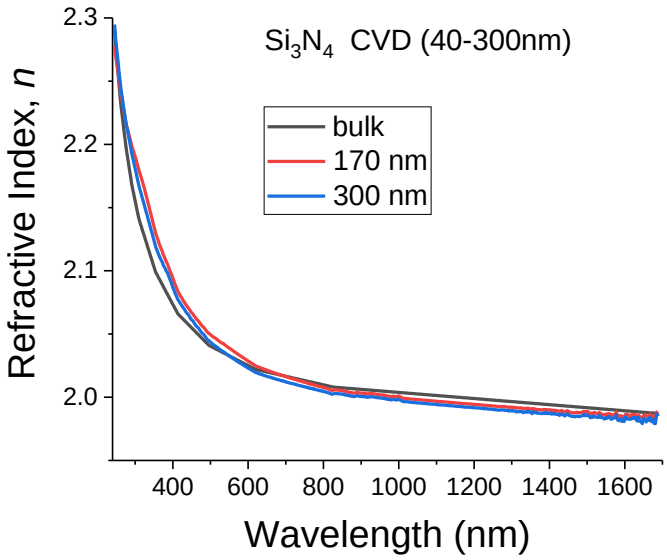

Figure S3. Spectral dependence of the refractive index of CVD Si_3N_4 film for different thickness.

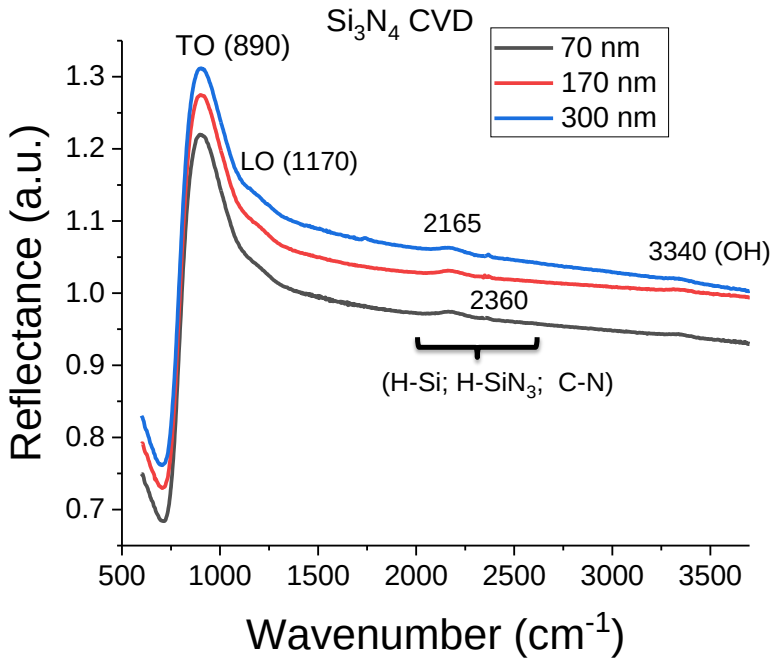

Figure S4. IR spectra of CVD Si_3N_4 film as a function of film thickness.

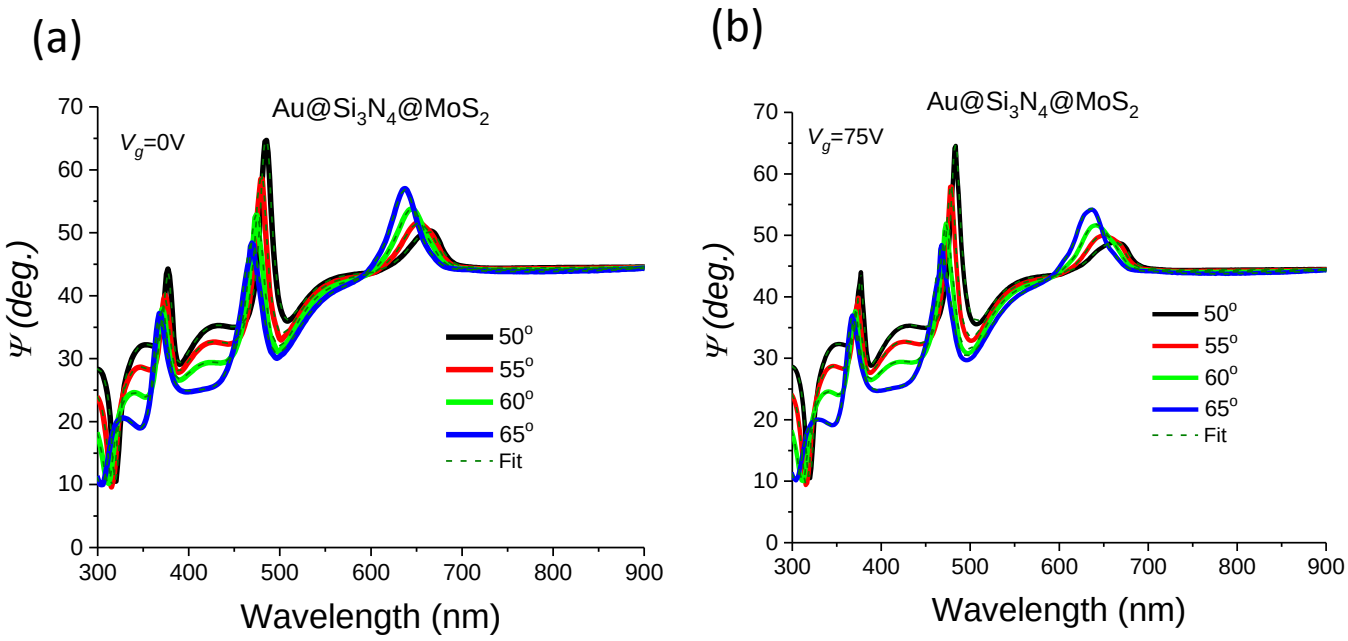

Figure S5. Spectral dependences of ellipsometric parameter Ψ observed at 50-65degs angles of incidence for $Au/Si_3N_4/MoS_2$ hybrid waveguide nanostructure. The measured (solid lines) and modeled (olive, dash) Ψ-spectra for different gate voltages (a) V_g=0V and (b) V_g=75V

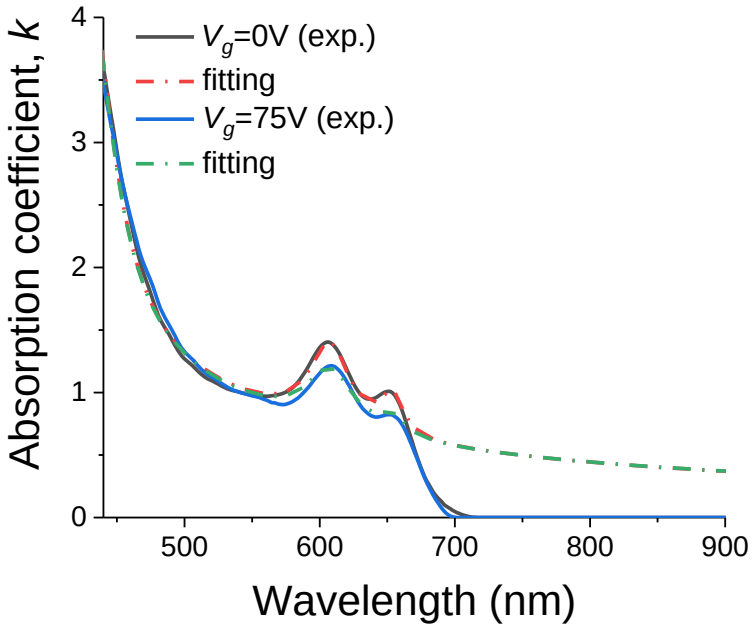

Figure S6. Measured and fitted imaginary part of the refractive index of monolayer MoS_2 film for different gate voltages.

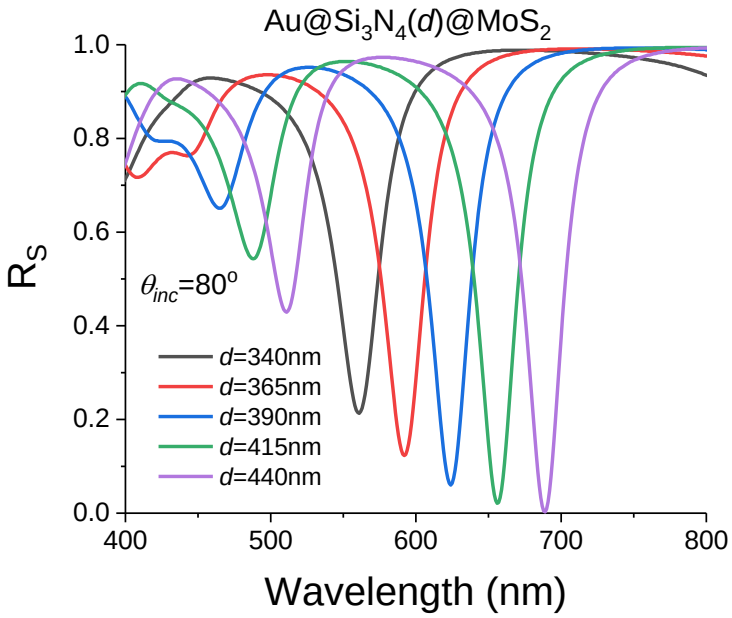

Figure S7. The calculated *s*-polarised reflection of the $MoS_2/Si_3N_4/Au$ nanostructure as a function of thickness of the dielectric Si_3N_4 film.